Journal of Biomedical Optics

SPIEDigitalLibrary.org/jbo

Photon budget analysis for fluorescence lifetime imaging microscopy

Qiaole Zhao
Ian T. Young
Jan Geert Sander de Jong

SPIE

Photon budget analysis for fluorescence lifetime imaging microscopy

Qiaole Zhao,[a] Ian T. Young,[a] and Jan Geert Sander de Jong[b]
[a]Delft University of Technology, Department of Imaging Science and Technology, The Netherlands
[b]Lambert Instruments, The Netherlands

Abstract. We have constructed a mathematical model to analyze the photon efficiency of frequency-domain fluorescence lifetime imaging microscopy (FLIM). The power of the light source needed for illumination in a FLIM system and the signal-to-noise ratio of the detector have led us to a photon "budget." These measures are relevant to many fluorescence microscope users and the results are not restricted to FLIM but applicable to widefield fluorescence microscopy in general. Limitations in photon numbers, however, are more of an issue with FLIM compared to other less quantitative types of imaging. By modeling a typical experimental configuration, examples are given for fluorophores whose absorption peaks span the visible spectrum from Fura-2 to Cy5. We have performed experiments to validate the assumptions and parameters used in our mathematical model. The influence of fluorophore concentration on the intensity of the fluorescence emission light and the Poisson distribution assumption of the detected fluorescence emission light have been validated. The experimental results agree well with the mathematical model. This photon budget is important in order to characterize the constraints involved in current fluorescent microscope systems that are used for lifetime as well as intensity measurements and to design and fabricate new systems. [DOI: 10.1117/1.3608997]

Keywords: fluorescence microscopy; fluorescence lifetime imaging microscopy; photon efficiency; signal-to-noise ratio; light power.

Paper 10496RRR received Sep. 10, 2010; revised manuscript received May 23, 2011; accepted for publication Jun. 16, 2011; published online Aug. 17, 2011.

1 Introduction

Fluorescence microscopy has become an essential tool in biology and medicine. Whether fluorescence intensity, color, lifetime, or any of the other properties that can be revealed (e.g., anisotropy) is being assessed, an understanding of the limitations induced by the observational instrumentation as well as the fluorescent process itself is necessary. We are developing a new generation of instrumentation for fluorescence lifetime imaging microscopy (FLIM) for reasons that will be described at the end of this manuscript. In this project, we have found it essential to develop a model that links the number of excitation photons, the number of emission photons, and the signal-to-noise ratio (SNR) that would be present in a resulting digital image when the fluorescence data are acquired through a digital microscope-based imaging system. Our resulting model, however, is equally applicable to widefield fluorescence microscopy in general. But we begin with FLIM.

After excitation by the absorption of a photon of a certain wavelength by a fluorescent molecule and barring its photodestruction, the molecule will be in an excited state. When the fluorophore returns to its ground state, a photon of a longer wavelength λ_{em}, compared to wavelength of the excitation photon λ_{ex}, is emitted. The fluorescence lifetime is the average time that a fluorophore remains in an excited state before returning to the ground state.[1] FLIM is a well-established and intrinsically quantitative tool to image the lifetime of fluorescent molecules. Unlike fluorescence intensity, the lifetime is independent of fluorophore concentration and light path length and can be used to investigate the environmental properties of the fluorescent molecule, such as pH, Ca^{++}, or O_2 levels.[2] Fluorescence lifetime imaging is, therefore, applied in a variety of biomedical fields.[3–8]

The estimation of the fluorescence lifetime can be divided into two major categories – time domain and frequency domain. In the time-domain method, a short light pulse, from a flash lamp or pulsed laser, is used to excite the fluorescent molecules under study, after which the emission is sampled in time so that the decay curve at every location in the image can be directly measured.[8–10] In the frequency-domain method, the fluorescent molecules are excited by modulated light, which is usually driven by a sinusoidal function of time with a certain frequency. By measuring the phase delay and/or the modulation depth of the fluorescence emission, the lifetime can be determined.[11–13] In practice, frequency-domain FLIM has specific advantages over time-domain FLIM despite the fact that in theory they are equivalent.[11]

To quantify the performance of a frequency-domain lifetime imaging technique, photon efficiency, or "economy" as described by Esposito et al.,[15] has been studied by many researchers and an F-value has been used to describe a "normalized relative root-mean-square noise."[14–17] Little attention, however, has been paid to the photon efficiency of the system. When Esposito et al. studied the relative throughput of a detection technique, the efficiency was considered to be 1,[15] which is normally not the case. In reality, many factors play a role in determining the system efficiency, such as the collection efficiency of an objective lens, the optical component light transmission

Address all correspondence to: Ian T. Young, Delft University of Technology, Department of Imaging Science & Technology, Lorentzweg 1, 2628 CJ Delft, The Netherlands; Tel: +31-15-278-5390; Fax: +31-15-278-6740; E-mail: i.t.young@tudelft.nl.

1083-3668/2011/16(8)/086007/16/$25.00 © 2011 SPIE

or reflection efficiency, the fill factor and quantum efficiency of the camera, and so on.[18,19] Clegg described the sensitivity of fluorescence measurement by listing some factors that require attention[20] but he did not provide a quantitative analysis. To better understand the constraints that are encountered in current and future microscope systems, a mathematical model has been developed to provide a quantitative photon budget analysis. In this photon budget, we focus on the choice of the light source for a FLIM system and the SNR that a camera should ultimately achieve. These subjects are relevant to many fluorescence microscope users and the results are not restricted to FLIM, but applicable to widefield fluorescence microscopy in general. Limitations in photon numbers, however, are more of an issue with FLIM compared to other less quantitative types of imaging. Considerations associated with fluorescence resonance energy transfer, however, are excluded. We have also performed experiments to validate the assumptions used in the mathematical model.

2 Theory

A fluorescence system, consisting of an ensemble of molecules, can be considered for the most part as a linear time-invariant (LTI) system.[21,22] It is linear because the weighted sum of two excitation signals will produce the weighted sum of two emission signals. Mathematically, if $x_1(t) \rightarrow y_1(t)$ and $x_2(t) \rightarrow y_2(t)$, then $\alpha x_1(t) + \beta x_2(t) \rightarrow \alpha y_1(t) + \beta y_2(t)$, in which α and β are scaling factors. The system can be considered as time-invariant until photo-destruction of the fluorescent molecules occurs. This means that a delay in the excitation signal $x(t - t_0)$ will produce a corresponding delay in the emission signal $y(t - t_0)$.

Since the fluorescence system is an LTI system with an impulse response characterized by the sum of one or more decaying exponentials, the fluorescence emission resulting from a sinusoidally-modulated excitation light source will also be modulated at the same frequency but with a phase shift and a decreased depth of modulation. The frequency-domain FLIM system uses a sinusoidally modulated light source and a detector modulated at the same frequency to calculate the lifetime. Note that the principle requirement is that the modulation and demodulation signals have the same Fourier harmonics. This allows, for example, the use of square-wave demodulation. A single lifetime can be calculated using Eq. (1) and/or Eq. (2) (Ref. 23)

$$\tau_\theta = \frac{1}{2\pi f_0} \tan(\Delta\varphi), \tag{1}$$

$$\tau_m = \frac{1}{2\pi f_0} \sqrt{\frac{1}{m_d^2} - 1}. \tag{2}$$

In Eqs. (1) and (2), $\Delta\varphi$ is the phase change, f_0 is the modulation frequency, and m_d is the relative modulation depth of the emission signal compared to the excitation signal. These two derived lifetimes are only equal to the true fluorescence lifetime for mono-exponential homogeneous lifetime samples. Often, however, the sample being measured contains various quantities of differing lifetime species or species in a multiplicity of lifetime states. When this occurs, the lifetimes derived from the phase and from the modulation depth will no longer be equal. In order to determine the lifetimes in the presence of two or more lifetime components, the phase and modulation must be recorded at multiple frequencies, where the reciprocal of the frequencies are, in general, chosen so as to span the full lifetime range in the sample (typically 10 to 100 MHz for nanosecond fluorescence lifetimes). A minimum of N frequency measurements is required to discern N lifetime components.[2]

In this section, we will discuss the mathematical model required to determine 1. the power of the light source and 2. the resulting SNR at the detector.

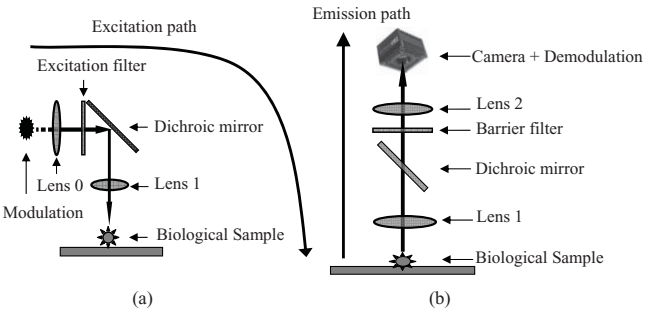

Fig. 1 Illustration of the schematic for the photon budget analysis. (a) Excitation path that is used to calculate the power of the light source and (b) emission path that is used to deduce the SNR at the detector.

2.1 *Estimating the Power of the Light Source*

A photon budget analysis describing the amount of light needed to excite a fluorescence sample is presented below. This analysis can be used to choose a suitable light source for a proposed FLIM system or for a (quantitative) fluorescence microscope system. Based on a hypothesized number of emission photons, the number of excitation photons is deduced by following the excitation path back to the light source, as shown in Fig. 1(a).

We assume that an $a \times a$ pixel camera is used, a square pixel size of $b \times b$ [meter^2], and a total optical magnification of M. The numerical aperture of the objective lens is NA. The excitation wavelength is λ_{ex} [meter]. The volume of the voxel, V, that is associated with each imaged pixel at the specimen will approximately be

$$V = (\Delta x)(\Delta y)(\Delta z) \approx \left(\frac{b}{M}\right)^2 \left(\frac{\lambda_{ex}}{2\mathrm{NA}^2}\right) [\mathrm{m}^3], \tag{3}$$

$$\Delta z \approx \frac{\lambda_{ex}}{2\mathrm{NA}^2}, \tag{4}$$

where Δz is the depth-of-field.[24] Assuming that the fluorescent molecule concentration c [mol/m^3] is given, there will then be m molecules per voxel

$$m = c\mathrm{N_A} \left(\frac{b}{M}\right)^2 \left(\frac{\lambda_{ex}}{2\mathrm{NA}^2}\right) [\mathrm{molecules/voxel}] \tag{5}$$

in which, $\mathrm{N_A} = 6.022 \times 10^{23}$ mol^{-1} is Avogadro's constant. If c is expressed as a molar solution [mol/liter], then the proper conversion to [mol/m^3] must be made.

Let us assume that each fluorescent molecule can emit n_{emit} photons before photo-destruction ends the fluorescence emission. One fluorescein molecule, for example, can emit

30,000 to 40,000 photons before it is permanently bleached.[25] The values for some other fluorescent molecules are given in Table 1. We can, therefore, expect to collect a maximum of $n_{emit} \cdot m$ photons per voxel. If the lifetime estimate requires the recording of r images, each of which takes T seconds, and the time interval between two recordings is identical and is T_0 seconds, then the average number of photons per recording will be

$$\begin{aligned} n_{rec} &= \frac{n_{emit} T m}{rT + (r-1)T_0} \\ &= \frac{n_{emit} T}{rT + (r-1)T_0} \left[c \mathrm{N_A} \left(\frac{b}{M} \right)^2 \left(\frac{\lambda_{ex}}{2\mathrm{NA}^2} \right) \right] \\ &\quad \times [\text{photons/recording/voxel}]. \end{aligned} \tag{6}$$

For the conventional application, widefield fluorescence microscopy, we set $r = 1$. We assume, but do not recommend, that the excitation light is left on during the $(r-1)T_0$ inter-recording intervals. If this is not the case and the excitation light is switched off, then we can set $T_0 = 0$ in Eq. (6). Excitation photons that enter a volume containing fluorophores are either absorbed within the volume or pass through it. It is not important to know by what mechanism they leave the volume, e.g., direct transmission or scattering. What is important is that they are not absorbed. We refer to the number of excitation photons entering the volume as n_0 and the number of emission photons exiting the volume as n_1. Not every absorbed photon produces an emission photon and the ratio emitted to absorbed is the quantum yield Φ, with typical values being $0.5 \leq \Phi \langle 1$. An ideal fluorophore would have a quantum yield close to unity.

Emission photons either leave the volume or they remain in the volume through re-absorption. Using Eqs. (5) and (6), the relation between 1. the net number of photons that are emitted from a volume and, thus, could be recorded in an image and 2. the photons that are (re)absorbed and, thus, do not leave the volume is given by

$$\begin{aligned} &\Phi n_{absorb} = \Phi (n_0 - n_1) = n_{rec} \text{ [photons/recording]} \Rightarrow \\ &n_{absorb} = \frac{n_{emit} T m}{[rT + (r-1)T_0]\,\Phi} \text{ [absorbed photons/recording]}. \end{aligned} \tag{7}$$

According to the Beer-Lambert law, we can relate the number of photons entering the volume n_0 to the number of photons leaving the volume by

$$n_1 = n_0 \times 10^{-A}, \tag{8}$$

where A is the absorption coefficient. Using Eqs. (4) and (5), the absorption coefficient A for one voxel path length Δz is

$$\begin{aligned} A &= \varepsilon(\lambda_{ex}) c \Delta z \\ &= \varepsilon(\lambda_{ex}) \left[\frac{m}{\mathrm{N_A} \left(\frac{b}{M} \right)^2 \left(\frac{\lambda_{ex}}{2\mathrm{NA}^2} \right)} \right] \left(\frac{\lambda_{ex}}{2\mathrm{NA}^2} \right) \\ &= \frac{\varepsilon(\lambda_{ex}) m M^2}{\mathrm{N_A} b^2}, \end{aligned} \tag{9}$$

where $\varepsilon(\lambda_{ex})$ [m^2/mol] is the molar extinction coefficient of the fluorescent molecule. The SI units for $\varepsilon(\lambda_{ex})$ are m^2/mol, but in practice, they are usually taken as M^{-1} cm^{-1}. The value of $\varepsilon(\lambda_{ex})$ depends on the excitation wavelength.

Our choice of a "volume" needs some elaboration. First, as we are using epi-illumination, a single microscope objective for the excitation path as well as the emission path, we assume that the volume of the sample that is being excited is the same as the volume that is observed for fluorescence. The approximate dimensions of this volume are the area in the lateral plane of one pixel $(b/M)^2$ and the value of Δz given in Eq. (4) in the axial path. The amount of intensity that is to be found in this volume compared to the total volume that is illuminated and examined is about 70%. This value follows from direct application of the theory described in Ref. 24, Sec. 8.8.3, Eq. (39).

Solving for the number of excitation photons needed to produce the number of absorbed photons per recording (r) gives

$$\begin{aligned} n_0 &= \left(\frac{1}{1 - 10^{-A}} \right) n_{absorb} \\ &= \frac{T m n_{emit}}{[rT + (r-1)T_0]\,\Phi (1 - 10^{-\frac{\varepsilon(\lambda_{ex}) m M^2}{\mathrm{N_A} b^2}})} \\ &\quad \times [\text{photons/recording}]. \end{aligned} \tag{10}$$

We use n_0 as the maximum value per voxel. If more excitation photons are used than this, then the molecules will bleach before the necessary number of recordings has been made.

As shown in Fig. 1, the reflection efficiency of the dichroic mirror R_D, the transmission efficiency of the excitation filter τ_{EF}, and the transmission efficiency of the lenses in the excitation path τ_{lens01} should also be considered. R_D, τ_{EF}, and τ_{lens01} are all wavelength dependent, but for notational simplicity we will forego using an explicit notation such as $R_D(\lambda)$. The number of photons from the light source needed to produce n_0 excitation photons will, therefore, be

$$\begin{aligned} n_{0source} &= \frac{n_0}{R_D \tau_{EF} \tau_{lens01}} \\ &= \frac{T m n_{emit}}{[rT + (r-1)T_0]\, R_D \tau_{EF} \tau_{lens01} \Phi (1 - 10^{-\frac{\varepsilon(\lambda_{ex}) m M^2}{\mathrm{N_A} b^2}})} \\ &\quad \times [\text{photons/recording/pixel}]. \end{aligned} \tag{11}$$

The number of excitation photons, $n(\lambda_{ex})$, per second required for illumination of the entire field of view (as opposed to just one pixel) will be

$$\begin{aligned} n_i(\lambda_{ex}) &= \frac{a^2 n_{0source}}{T} \\ &= \frac{a^2 m n_{emit}}{[rT + (r-1)T_0]\, R_D \tau_{EF} \tau_{lens01} \Phi (1 - 10^{-\frac{\varepsilon(\lambda_{ex}) m M^2}{\mathrm{N_A} b^2}})} \\ &\quad \times [\text{photons/s/image}]. \end{aligned} \tag{12}$$

If the energy from the light source is E_{ex} [J/photon], then the power W of the light source required for excitation of the entire

Table 1 Light power needed to produce the maximum number of emission photons from a single fluorescent molecule in 0.2 s. The values have been calculated for nine different fluorophores whose absorption peaks span the visible spectrum. The calculations are based upon the data in this table and Eq. (13). As the maximum number of emission photons is a statistical average over an ensemble of identical molecules, all values are averages. (§This value is estimated from Ref. 25.)

Fluorophore	Maximum number of photons per molecule	Molar extinction coefficient $[M^{-1}cm^{-1}]$	λ_{ex} Peak [nm]	λ_{em} Peak [nm]	Quantum yield Φ	Light source power [mW]	References
Fura-2	250	2.19×10^4	380	512	0.50	0.2	31,32
GFP	4×10^5	4.4×10^4	446	509	0.77	94	33–35
Fluorescein	3×10^4	5.97×10^4	494	525	0.90	5	25,28,29
EYFP	10^5 (§)	8.34×10^4	514	527	0.61	14	25,35,36
Rhodamine 6G	1.1×10^6	1.16×10^5	530	555	0.95	67	37–39
Alexa546	3.5×10^6	1.12×10^5	561	572	0.79	250	35,37,40
Cy3	4.8×10^6	1.25×10^5	550	570	0.15	1.7×10^3	35,37,41
Tetramethylrhodamine	1.2×10^6	1×10^5	550	573	0.71	109	37,42,43
Cy5	9.9×10^4	2.5×10^5	650	666	0.23	9	35,44,45

field of view is

$$W = n_i E_{ex} = \frac{a^2 m n_{emit} E_{ex}}{[rT + (r-1)T_0]\, R_D \tau_{EF} \tau_{lens01} \Phi (1 - 10^{-\frac{\varepsilon(\lambda_{ex}) m M^2}{N_A b^2}})} \times [\text{Watts}]. \quad (13)$$

2.2 *Estimating the Signal to Noise Ratio at the Detector*

We can identify four possible noise sources for digitized fluorescence images: photon noise due to the fundamental (quantum) physics of photon production (P), dark current noise due to the production of photoelectrons through thermal vibrations (D), readout noise due to the analog and digital electronics (E), and quantization noise due to the process of converting an analog intensity value into a quantized gray level (Q). These noise sources are mutually independent and this means that the total noise variance $\sigma^2{}_T$ is the sum of each of the noise variances: $\sigma^2{}_T = \sigma^2{}_P + \sigma^2{}_D + \sigma^2{}_E + \sigma^2{}_Q$. Through cooling, as with a Peltier element, and short integration times (in our case this is about 200 ms), the dark current contribution, $\sigma^2{}_D$, can be neglected, that is $\sigma^2{}_D \approx 0$. Through proper electronics design the readout contribution, $\sigma^2{}_E$, can be neglected. The analog-to-digital convertor (ADC) readout noise, for example, is dependent on the ADC readout frequency (in our system it is 11 MHz), and is, thereby, reduced to manageable levels, that is $\sigma^2{}_E \approx 0$.

This leaves the contributions from photon noise and quantization noise, $\sigma^2{}_T = \sigma^2{}_P + \sigma^2{}_Q$. We begin with photon noise and denote the signal-to-noise ratio for photon noise as simply SNR.

The SNR at the detector is calculated by analyzing the photon loss in the emission path, as shown in Fig. 1(b). We assume that the total number of photons that a single fluorescent molecule can emit before photo-destruction occurs is n_{emit}. Allowing r phase recordings, each of which takes T seconds, and the time interval between two recordings as T_0 seconds, n_{epr} photons are emitted on average and thus can be used per recording

$$n_{epr} = \frac{n_{emit} T}{[rT + (r-1)T_0]} [\text{usable photons/recording}]. \quad (14)$$

But not all of these photons will be collected by the objective lens. The numerical aperture (NA) describes the light collection ability of a lens and is given by

$$\text{NA} = n \sin\theta, \quad (15)$$

in which θ is the acceptance angle of the lens and n is the index of refraction of the immersion medium of the lens. The number of photons, which have the chance to reach and be captured by the lens (n_{lens}) is dependent upon θ.

Figure 2(a) illustrates the isotropic emission of fluorescence photons and the fraction captured by the objective lens. The number of photons that can be captured by the lens n_{lens} within an angle θ is

$$n_{lens} = n_{epr}(1 - \cos\theta)/2. \quad (16)$$

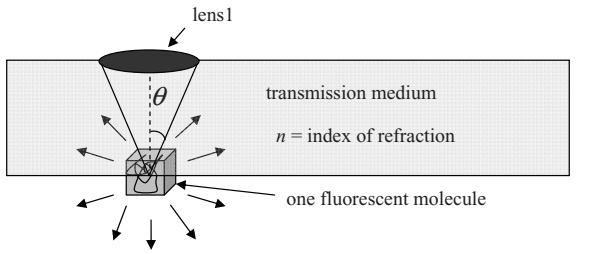

(a)

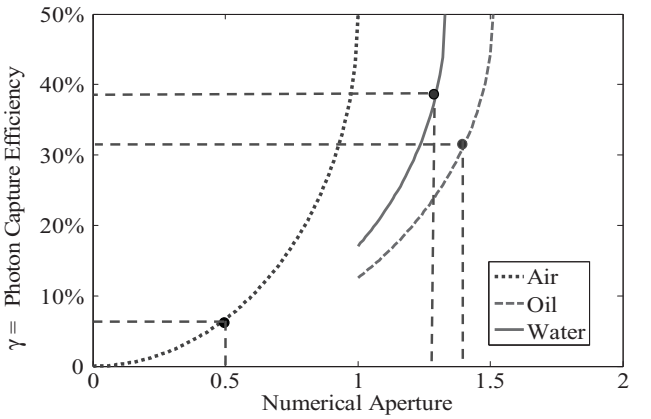

(b)

Fig. 2 Photon-capture efficiency of the objective lens. (a) Illustration of the directions of photons emitted by a fluorescent molecule and that portion captured by the objective lens. (b) Fraction of photons captured by various lenses compared to the photons emitted by one fluorescent molecule. If the immersion medium is air $n = 1$, $0 \le \text{NA} \le 1$; if it is water, $n = 1.33$, NA $\rangle$ 1; and if it is immersion oil, $n = 1.51$, NA $\rangle$ 1. Values for different objective lenses (Nikon, Fluor Ph2DL,10×, NA0.5; Nikon, Plan Fluor 100×, NA 1.3; Zeiss, Plan, 63×, NA1.4) are marked as dots in the figure.

The factor of 1/2 in Eq. (16) comes from the fact that only half of the isotropically emitted photons travel toward the lens. The photon capture efficiency γ of the lens is described in Eq. (17) and is the photon number that the lens can capture divided by the total number of photons that the fluorescent molecules emit. Figure 2(b) shows the photon capture efficiencies for different immersion media such as air ($n = 1.0$), water ($n = 1.33$), and oil ($n = 1.51$). Typical values of different lenses are marked as dots in Fig. 2

$$\gamma = \frac{n_{lens}}{n_{epr}} = \frac{1 - \cos\theta}{2} = \frac{1 - \sqrt{1 - \sin^2\theta}}{2} = \left[1 - \sqrt{1 - (\text{NA}/n)^2}\right]/2. \quad (17)$$

The transmission efficiencies of the objective lens, the dichroic mirror, the barrier filter, and the second lens are denoted τ_{lens1}, τ_D, τ_B, and τ_{lens2}, respectively. The transmission coefficient of the camera window is τ_w, the fill factor is F, and the quantum efficiency is η. The parameters τ_{lens1}, τ_D, τ_B, τ_{lens2}, τ_w, and η are emission wavelength dependent but again, we suppress the functional dependency on λ in favor of notational simplicity. The ratio of the CCD area to the excitation spot area is κ. Then the number n_e of photoelectrons detected

by the camera will be

$$n_e(\lambda) = \underbrace{(\tau_{lens1}\tau_D\tau_B\tau_{lens2}\tau_w\eta)}_{wavelength\ \ dependent}\kappa F n_{epr}(\lambda) \times \left[1-\sqrt{1-(\mathrm{NA}/n)^2}\right]/2. \quad (18)$$

We assume in this manuscript, for the sake of simplicity, that the terms in Eq. (19) that vary over the emission wavelengths of interest, ($\lambda_1 \le \lambda \le \lambda_2$), can be replaced by zeroth-order (constant) terms. We are essentially appealing to the mean value theorem of calculus. This allows us to go from line two to lines three and four in Eq. (19). The total number of photoelectrons would then be given by

$$\begin{aligned} n_e &= \int_0^\infty n_e(\lambda)d\lambda \\ &= \left(\int_0^\infty \tau_{lens1}\tau_D\tau_B\tau_{lens2}\tau_w\eta n_{epr}(\lambda)d\lambda\right) \\ &\quad\times\left\{\kappa F\left[1-\sqrt{1-(\mathrm{NA}/n)^2}\right]\Big/2\right\} \\ &= (\tau_{lens1}\tau_D\tau_B\tau_{lens2}\tau_w\eta)\underbrace{\left(\int_{\lambda_1}^{\lambda_2} n_{epr}(\lambda)d\lambda\right)}_{n_{epr}} \\ &\quad\times\left\{\kappa F\left[1-\sqrt{1-(\mathrm{NA}/n)^2}\right]\Big/2\right\} \\ &= (\tau_{lens1}\tau_D\tau_B\tau_{lens2}\tau_w\eta)\left\{\kappa F\left[1-\sqrt{1-(\mathrm{NA}/n)^2}\right]\Big/2\right\}n_{epr}. \end{aligned} \quad (19)$$

Two remarks are appropriate. First, as described by Roper Scientific and Andor Technology, the quantum efficiency of a standard, front-illuminated CCD chip over the FWHM emission wavelength range of green fluorescent protein (GFP) (496 nm $\le \lambda \le$ 524 nm), can be extremely well approximated by η = 24% over this entire interval. Other "special" CCD chips such as those used by the Santa Barbara Instrumentation Group can be well approximated by η = 71% over this interval. Thus, the value of η may vary from chip-to-chip but the use of a constant value over the wavelength interval for a given chip is justified.

Second, and perhaps more importantly, the term n_{epr} in Eq. (19) represents the number of emission photons within the range ($\lambda_1 \le \lambda \le \lambda_2$), a number that is dependent upon the emission spectrum of the fluorescent molecule and the barrier and dichroic filters. For our GFP example, where λ_1 = 502 nm and λ_2 = 538 nm (see filter and experiment descriptions below), approximately 61% of the emitted photons are within this wavelength range.

Assuming the number of photons recorded during a fixed measuring period is random and described by a Poisson distribution,[26] the SNR is defined and given by Ref. 27

$$\begin{aligned} SNR &= \frac{\text{average}}{\text{std. deviation}} = \frac{\mu}{\sigma} \\ &= \frac{\langle n_e\rangle}{\sqrt{\langle n_e\rangle}} = \sqrt{\langle n_e\rangle} \\ &= \left\{\frac{(\tau_{lens1}\tau_D\tau_B\tau_{lens2}\tau_w\eta F\kappa)\,T n_{emit}\left[1-\sqrt{1-(\mathrm{NA}/n)^2}\right]}{2\,[rT+(r-1)T_0]}\right\}^{1/2}. \end{aligned} \quad (20)$$

When expressed in the logarithmic units commonly used for electro-optics, this becomes SNR = $20\log_{10}(\mu/\sigma) = 10\log_{10}(n_e)$ dB. A more rigorous calculation of the SNR would involve taking the wavelength dependency of the various terms in Eq. (20) into consideration, that is, performing an integration over the relevant wavelengths. The terms τ_D, τ_B, and n_{emit} have the most significant variations as a function of wavelength but for this analysis, as explained above, we use the simplest approximation of their being constant.

The average of n_e ($\langle n_e\rangle$) is calculated over the CCD pixels. With an electronic gain g [ADU/e], the conversion of photoelectrons to A/D converter units N [ADU] is described by $N = gn_e$. The average and standard deviation of N can be easily obtained: $\langle N\rangle = g\langle n_e\rangle$, $\sigma(N) = g(\langle n_e\rangle)^{1/2}$. Thus, the SNR after conversion is the same as that before conversion, which indicates that the ADC conversion factor does not change the fundamental SNR, but only the observed gray level dynamic range.

There is a slight amount of quantization noise introduced by the ADC but that noise is, in general, negligible when compared to photon noise from fluorescence. The reasoning is as follows. Without loss of generality, the signal can be normalized to the interval 0 $\le$ signal $\le$ 1. This is quantized into 2^b uniformly spaced intervals each of width $q = 2^{-b}$, where b is the number of bits. Replacing the analog value with the digitized value is equivalent to adding uniformly-distributed noise to the original value where the noise distribution has a mean of 0 and a variance of $\sigma^2_Q = q^2/12$. The SNR_Q for this signal is defined as SNR_Q = (max signal)/σ_Q = $sqrt(12)$/q = $sqrt(12)2^b$. Rewriting this in logarithmic (dB) form gives $\mathrm{SNR}_Q = 6b + 11$ dB.[27] For a 10-bit ADC, the SNR_Q = 71 dB. This is much higher than

the typical SNR per pixel and can thus be ignored leaving the photon noise as the limiting factor.

3 Materials and Methods

3.1 *System Configuration*

Our baseline FLIM system includes an Olympus inverted microscope system IX-71 (Olympus), a LIFA system (Lambert Instruments, Roden, The Netherlands), a LI^{2}CAM intensified CCD camera (Lambert Instruments, Roden, The Netherlands), and a Dell computer installed with the Windows XP operating system.

A Zeiss objective with a magnification of 20× and a numerical aperture of 0.5 has been used. The lateral resolution associated with the GFP emission wavelength is $\lambda_{em}/(2NA) = 509$ nm and the axial resolution is $\lambda_{em}/(2\ NA^2) = 1018$ nm. The dependence of the SNR on the NA is explicitly given in Eq. (20). Our LIFA system uses LED excitation with an emission peak at $\lambda = 469$ nm (Lambert Instruments, Roden, The Netherlands) in combination with a 472 ± 15 nm single-band excitation filter (Semrock FF01-472/30-25, Rochester, New York). A 495-nm LP dichroic mirror (Semrock FF495-Di02-25 × 36, Rochester, New York) is used in the fluorescence filter cube. The fluorescence is observed through a 520 ± 18 nm single-band emission filter (Semrock FF01-520/35-25, Rochester, New York).

The LED DC current setting, via LI-FLIM software version 1.2.6 developed by Lambert Instruments, controls the intensity of the LED. Light power is measured using a laser power meter Ophir Model No. PD-300-SH (Jerusalem, Israel).

3.2 *Materials*

To determine the effect of the fluorophore concentration on the emission light, Rhodamine 6G (Sigma Aldrich 83697) was diluted in deionized water to different concentrations: 10, 50, 100, 250, 500, 1000, and 2500 μM. Rhodamine was held between a single well pattern microscope slide (Fisher Scientific 361401) and a cover slip (Menzel-Gläser 18 mm × 18 mm). For the focus of the Rhodamine 6G solution, we 1. focus on the edge of the solution, 2. move the sample so that the middle of the solution sits above the objective pupil, and then 3. move the focus point into the solution by 50 μm using the indexed focusing knob.

A green fluorescence plastic test slide (Lambert Instruments) is used for validating the Poisson distribution assumption of the detected emission light, in order to avoid photobleaching either a biological sample or a fluorophore solution.

3.3 *Determining the Power of the Light Source*

Let us look at some typical values and take fluorescein as an example. We have chosen fluorescein because, as shown in Table 1, it is almost a worst-case example. It provides a relatively small number of emission photons before photo-destruction. The total number of photons that a single fluorescein molecule can emit before photo-destruction occurs is $n_{emit} \approx 30{,}000$.[25] Fluorescein has a molar extinction coefficient of $\varepsilon(\lambda_{ex}) = 59{,}668$ $M^{-1}cm^{-1}$ at 488 nm excitation light.[28] The quantum yield is $\Phi = 0.9$.[29] We assume a molecular concentration of $c = 2\ \mu$M. Further, we assume that an $a \times a = 512 \times 512$ pixel camera is used with a square pixel size of $b = 25\ \mu$m and a total optical magnification of $M = 100\times$. We assume that at the wavelengths of interest, the reflection efficiency of the dichroic mirror is $R_D = 95\%$, the transmission efficiency of the excitation filter is $\tau_{EF} = 95\%$,[30] and the transmission efficiency of the lenses in the excitation path are $\tau_{lens01} = 96\% \times 96\% \approx 92\%$. The numerical aperture NA = 1.3. A monochromatic 488-nm laser source is assumed for the excitation source. Allowing $r = 12$ different phase recordings, one recording takes $T = 200$ milliseconds, and the time interval between two measurements is $T_0 = 0$ s.

If we were to consider fluorescent molecules other than fluorescein, then the relevant fluorophore parameters needed to calculate the light power or SNR would be those given in Table 1. The equations and their derivations associated with some of the values in Table 1 and the following will be discussed in Sec. 4.1. Table 1 should be used with care as it presents the optical power required if one wants to extract every possible emission photon from a molecule. If a fewer number of photons is required to achieve a desired goal—measurement of fluorescence lifetime with a certain precision, for example—then a lower power light source could suffice.

3.4 *Determining the Signal to Noise Ratio at the Detector*

Using Eqs. (14)–(20), the number of photoelectrons that can be ultimately detected in FLIM can be calculated. We assume, for example, a NA = 1.3 objective lens with oil as the medium for which the index of refraction is $n = 1.51$. Continuing with the fluorescein model, the quantum efficiency of the camera system, which depends upon the wavelength, is about $\eta(\lambda \approx 525\ \text{nm}) \approx 30\%$. We assume the camera fill factor $F = 40\%$, the transmission efficiency of the dichroic mirror is $\tau_D = 90\%$, and that of the barrier filter is $\tau_B = 95\%$.[30] We assume the transmission of both lenses and the camera window are $\tau_{lens1} = \tau_{lens2} = \tau_w = 96\%$ and that the total number of photons that a single fluorescent molecule can emit is $n_{emit} \approx 30{,}000$. We assume the total phase recording number $r = 12$, and there is no time interval between two recordings $T_0 = 0$. If an $a \times a$ pixel camera is used and the diameter of the excitation circular spot is the same as the diagonal of the CCD chip, $\kappa = 2/\pi$. In reality the diameter of the excitation spot will be larger than the diagonal of the CCD chip, so we make an approximation that $\kappa = 1/2$.

To calculate the SNR for other fluorophores, the critical parameters that may need to be changed are the total number of photons that a single molecule can emit before photo-destruction occurs and the quantum efficiency of the camera system at a possibly different emission wavelength. Such values are shown in Table 2. The derivation will be discussed in Sec. 4.2.

3.5 *Assumptions and Parameter Validation*

We have performed a series of experiments to validate the parameter values and assumptions used in our photon efficiency model. Considering the transmission efficiency of the optical components (filters and lens) as a single constant factor in the mathematical model is reasonable but will be tested. The influence of dye concentration on the intensity of the fluorescence emission light and the Poisson distribution assumption

Table 2 Using Eq. (20) the SNR at the detector is calculated for the nine different fluorophores from Table 1. The SNR is evaluated for a single molecule and at a concentration of $c = 2\ \mu$M for a single pixel and for an entire 512×512 image. As in Table 1, all values are averages. ([§]This value is estimated from Ref. 25.)

Material	Maximum number of photons per molecule	λ_{em} peak [nm]	Camera quantum efficiency @ λ_{em}	SNR per molecule	SNR for a pixel ($c = 2\ \mu$M)	SNR for an image ($c = 2\ \mu$M)	References
Fura-2	250	512	0.3	0.5 : 1 (–6 dB)	1.4 : 1 (3 dB)	7×10^2 : 1 (57 dB)	31,47,48
GFP	4×10^5	509	0.3	19 : 1 (26 dB)	61 : 1 (36 dB)	3×10^4 : 1 (90 dB)	33,47,48
Fluorescein	3×10^4	525	0.3	5 : 1 (14 dB)	18 : 1 (25 dB)	9×10^3 : 1 (79 dB)	25,47,48
EYFP	10^5 ([§])	527	0.3	10 : 1 (20 dB)	32 : 1 (30 dB)	2×10^4 : 1 (84 dB)	25,47,48
Rhodamine 6G	1.1×10^6	555	0.35	35 : 1 (31 dB)	120 : 1 (42 dB)	6×10^4 : 1 (96 dB)	37,47,48
Alexa546	3.5×10^6	572	0.38	64 : 1 (36 dB)	222 : 1 (47 dB)	1×10^5 : 1 (101 dB)	37,47,48
Cy3	4.8×10^6	570	0.38	75 : 1 (38 dB)	260 : 1 (48 dB)	1×10^5 : 1 (102 dB)	37,47,48
Tetramethylrhodamine	1.2×10^6	573	0.38	38 : 1 (31 dB)	130 : 1 (42 dB)	7×10^4 : 1 (96 dB)	37,47,48
Cy5	9.9×10^4	666	0.5	12 : 1 (22 dB)	46 : 1 (33 dB)	2×10^4 : 1 (88 dB)	44,47,48

of the fluorescence emission light must certainly be validated. Standard Köhler illumination is used in these experiments.

3.5.1 *Transmission efficiency of the optical components*

In the mathematical model, the transmission efficiency of the optical components is treated as a constant parameter. To validate this, we measure the light at the source and the light exiting from the objective lens using the laser power meter. The LED DC current was varied from 10 to 150 mA. The power of the light coming out of the objective lens was then divided by the power of the light at the source to determine the transmission efficiency of the optical component chains.

3.5.2 *Influence of concentration on the detected fluorescence emission intensity*

In estimating the required power of the light source, we assume that the Beer-Lambert law describes the relation between excitation photon number and emission photon number as shown in Eq. (8). To express Eq. (8) in another way, the fluorescence emission photon number n_{rec} equals the product of the excitation photon number n_0 and an absorption factor $(1 - 10^{-c\epsilon\Delta z})$, as shown in Eq. (21)

$$n_{rec} = \Phi n_{absorb} = \Phi n_0(1 - 10^{-c\varepsilon\Delta z}) = B(1 - 10^{-cD}). \tag{21}$$

B is proportional to the power of the excitation light, which is controlled by the LED DC current setting; D is the product of the molar extinction coefficient and the absorption path length, $D = \varepsilon\Delta z$.

We performed a series of experiments under different sample concentrations in order to validate the applicability of the Beer-Lambert law. Rhodamine 6G (Sigma Aldrich 83697) was dissolved in deionized water and the concentrations of 10, 50, 100, 250, 500, 1000, and 2500 μM were used. The power of the excitation light was measured by the power meter adjusted for the peak wavelength of the LED source, $\lambda = 469$ nm. The power of the excitation light, which exited from the objective onto the sample, was 0.19, 0.36, 0.53, 0.70, and 0.87 mW, respectively. This is shown in Fig. 3(a). The power of the excitation light measured adjacent to the light source was 0.45, 0.85, 1.23, 1.62, and 2.00 mW, respectively. The ratio between the light coming out from the objective and that coming out from the light source is around 43%. The positions of the solution slides were maintained the same throughout the experiments so that the absorption path lengths would be the same. As only Rhodamine 6G solutions were used in the experiments, the molar extinction coefficient was not changed. In another words, D was held constant.

3.5.3 *Poisson distribution of the detected fluorescence emission light*

As a discrete probability distribution, the Poisson distribution describes the probability of a number of independent events (e.g., photon emissions) occurring in a fixed period of time on the condition that these events occur with a known average rate and independently of the time since the last event. The Poisson

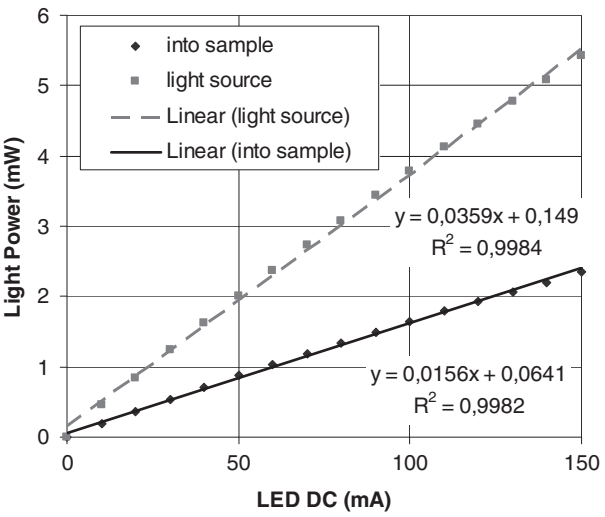

(a)

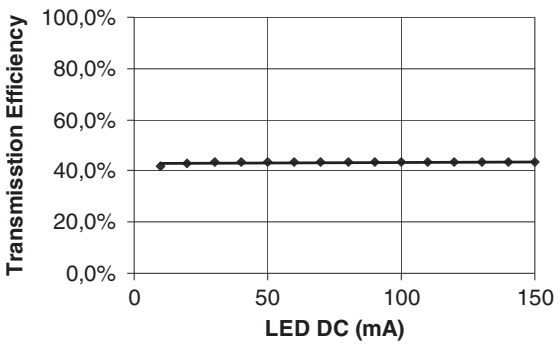

(b)

Fig. 3 Validation of the linearity of the entire measurement system and the constancy of the transmission efficiency of the optical components. (a) Light at the light source and the light exiting from the objective lens as the LED DC current is varied from 10 to 150 mA. Note that measured power is linear with the LED current. (b) Transmission efficiency of the optical component. Note that the efficiency is constant as a function of LED current.

distribution is given as

$$p(n|\mu) = \frac{\mu^n e^{-\mu}}{n!} \quad n = 0, 1, 2, 3, \ldots. \tag{22}$$

The expected number of photons that occur during the given interval is μ and the number of random occurrences of an event is n. Two important properties of the Poisson distribution [as used in Eq. (20)] are: 1. the average number of occurrences equals μ, i.e.,$\langle\, n\,\rangle = \mu$, and 2. the variance is also equal to μ, that is, $\sigma_n{}^2 = \langle\, (n-\mu)^2\,\rangle = \mu$.

In order to avoid photobleaching in a biology sample or a fluorophore solution, a green fluorescent plastic test slide (Lambert Instruments) was used in this measurement. Two images (i_1 and i_2) were consecutively taken with the microscope focused on the same place on the green fluorescent plastic slide under controlled LED DC current settings. The signal levels (per pixel) in these two images are denoted n_1 and n_2. We now look at the difference between these two images, which represents the difference of two independent samples of one random process.

This gives

$$\langle n_1 - n_2 \rangle = \langle n_1 \rangle - \langle n_2 \rangle = 0. \quad (23)$$

In words, the mean value of the difference should equal the difference of the mean values per pixel in the two images. This, in turn, is zero as the two images were taken under the same LED DC current setting [Eq. (23)] and, thus, represent independent samples of the same random process.

The variance, however, equals the sum of the two noise variances per pixel in the two independent images [Eq. (24)]. Until now, we have made no use of an explicit distribution for the light intensities other than that they have a mean and variance. If we now assume that the distribution of the number of emitted photons is Poisson, then we can make use of the explicit values for the mean and variance of such a process. Repeating the acquisition of pairs of images under differing intensities by varying the LED DC current settings (10 to 50 mA), this variance should be twice the average intensity

$$\sigma^2_{n_1-n_2} = \sigma^2_{n_1} + \sigma^2_{n_2} = 2\sigma^2_n = 2\mu. \quad (24)$$

4 Results and Discussion

4.1 *Power of the Light Source*

If we assume a fluorescein molecule concentration of approximately $c = 2\ \mu$M, then there are $m \approx 11$ molecules per voxel [see Eq. (5)]. Allowing $r = 12$ phase recordings, each of which takes $T = 200$ milliseconds, and the time interval between two recordings is $T_0 = 0$ s, $n_{rec} = (30{,}000 \times 11)/12 = 27{,}500$ photons per recording can be used as a maximum value per voxel [Eq. (6)]. Absorbance $A = 1.74 \times 10^{-6}$ over one voxel path length [Eq. (9)]. We find that $n_0 = 7.61 \times 10^9$ excitation photons per voxel per recording are needed to obtain 3.06×10^4 absorbed excitation photons [Eq. (10)]. The number of photons $n_{0source}$ we need from the light source will then be 9.15×10^9 [Eq. (11)].

If one recording takes 200 milliseconds, we have a maximum of $n_i = 512 \times 512 \times 9.15 \times 10^9/0.2 = 1.2 \times 10^{16}$ photons per second for illumination of the entire field of view [Eq. (12)]. This means a monochromatic 488 nm laser source ($= 4.07 \times 10^{-19}$ J/photon) with an optical power of about 5 mW is required for excitation of the entire sample [Eq. (13)]. At the sample plane, the optical power that will be delivered at $\lambda = 488$ nm is given by $W_{sp} = (R_D \tau_{EF} \tau_{lens01})W = (0.87)5$ mW $= 4.3$ mW [from Eq. (13)]. The validity of the assumptions used in the model will be discussed later in this paper.

Using the same method, the needed excitation powers are given in Table 1 for other molecules, assuming that the parameters found in the literature are correct. If we require a certain SNR to achieve a required measurement precision for a parameter such as fluorescence lifetime, it might not be necessary to use the maximum number of photons. If, for example, a measurement precision of 1% is reached with half the number of photons that a molecule is capable of producing, then there is no need to use further illumination.

4.2 *Signal to Noise Ratio at the Detector*

Using Eq. (18) for one molecule, approximately 27 photoelectrons can be collected per image by the camera per phase recording when the total phase recording number $r = 12$. For every 100 emission photons, $n_e/n_{epr} \approx 1\%$ [Eq. (18)], which means that approximately one photon will be converted into a photoelectron. The SNR before ADC conversion will be SNR $\approx 27/(27)^{1/2} \approx 5{:}1 \approx 14$ dB [Eq. (20)]. With an electronic gain for the camera of $g = 0.126$ [ADU/e$^-$],[26] an ideal estimation of the SNR for one molecule in an image is 5 (14 dB), which is good enough to eliminate the need for an electron multiplication (EM) readout for a charge-coupled device (CCD) camera system. By ideal we mean that, assuming all other noise sources are negligible, the SNR will only be limited by the Poisson-distributed, quantum photon noise. In the case of 15 dB or better, a typical high-end CCD without EM register performs better than a typical high-end EM-CCD, which adds multiplication noise.[46] But, should the excitation source be weaker, the quantum yield or the molar extinction coefficient be significantly lower, or the CCD be less sensitive to the emission wavelength, then EM could be required.

The SNR above is for one molecule in an image. Using a realistic estimate for a typical number of molecules (11 molecules per voxel), the power of a light source needed for FLIM is about 5 mW, and the expected SNR for a single camera pixel and for an entire image are 18:1 (25 dB) and 9000:1 (79 dB), respectively.

Using the parameter values found in the literature, the SNR for other fluorophores can be calculated, leading to the results shown in Table 2. In Table 2, we present the SNR for 1. a single molecule, 2. a single pixel at a fluorophores concentration of $c = 2\ \mu$M, and 3. an entire image at a concentration of $c = 2\ \mu$M.

4.3 *Assumption and Parameter Validation*

4.3.1 *Transmission efficiency of the optical components*

The results in Fig. 3(a) show that the system is linear, the light power both at the source and at the exit pupil of the objective lens linearly increase with an increased DC current to the LED. By dividing the light power at the exit pupil of the objective lens with the light power at the light source, the transmission efficiency of the optical component chains remains a constant, as shown in Fig. 3(b). The transmission efficiency (43%) is not high in this case due to the measurement configuration required for the laser power meter. A constant fraction of the photons was blocked before they could reach the exit pupil of the objective lens. But as the results show, we can treat the transmission efficiency of the optical components as a constant parameter in the mathematical model. Further, Fig. 3(a) tells us what current levels are required to achieve a given power level, W_{sp}, at the sample plane.

4.3.2 *Influence of concentration on the fluorescence emission intensity*

Figure 4(a) shows the fluorescence emission light power as a function of solution concentration. Each data point is the average of three measurements for a given Rhodamine 6G concentration [μM] and LED current [mA]. The experimental data

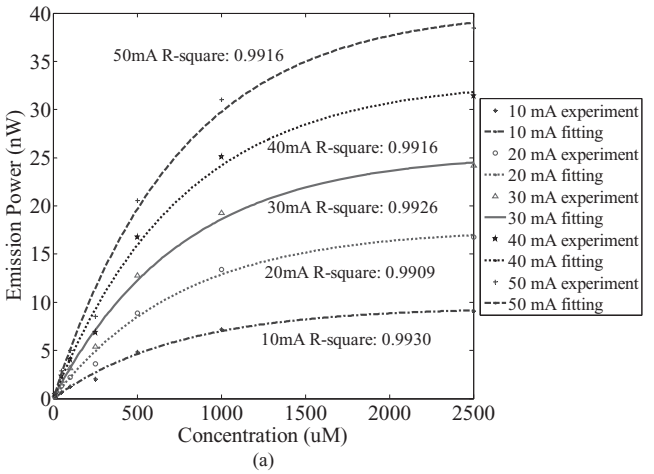

Fig. 4 Influence of sample concentration, c [μM], on the fluorescence emission intensity. (a) Fluorescence emission light power as a function of solution concentration for different LED current settings; (b) measured intensity parameter B from Eq. (21) as a function of LED DC current averaged over the seven different concentrations; and (c) product of molar extinction coefficient and the absorption path length D from Eq. (21) averaged over the seven different concentrations.

under differing LED DC current settings and differing concentrations fit well with the model in Eq. (21), the R-squared values are 0.9930, 0.9909, 0.9926, 0.9916, and 0.9916 under 10, 20, 30, 40, and 50 mA LED DC current, respectively. Figure 4(b) is a plot of the value of B found by fitting Eq. (21) to the data averaged over all seven concentrations (10, 50, 100, 250, 500, 1000, and 2500 μM) under different LED DC current settings. This shows that the measured intensity parameter B is linearly related to the LED DC current. Figure 4(c) is a plot of the value of D found by fitting Eq. (21), again, averaged over the seven concentrations at each of the LED DC current settings. Figure 4(c) shows that D remains the same and is independent of the emission intensity as we expect. We conclude that the Beer-Lambert law is appropriate for obtaining the absorption factor over the range of Rhodamine 6G concentrations used here.

4.3.3 *Poisson distribution of the detected fluorescence emission signal*

The experimental results are shown in Fig. 5. Using the LED DC current setting at 10 mA as an example, Fig. 5(a) shows one of the two images acquired from the green fluorescent plastic sample. The difference between the two images, caused by the random noise, is shown in Fig. 5(b). By varying the LED DC current setting from 10 to 50 mA, the mean and the variance of the difference image for a given current setting can be plotted as a function of the LED DC current value. Figure 5(c) shows that the mean value of the difference image under different current settings is close to zero as predicted in Eq. (23). Figure 5(d) shows that the variance of the difference images linearly increases with the LED DC current value, as expected. Together, they validate the Poisson distribution assumption used in the mathematical model.

4.3.4 *Final validation*

The models and their associated equations given above have produced a variety of predictions for light source strength and SNR for varying fluorophores. The experiments presented above are intended to validate these models by testing measured values against predictions.

We have performed additional experiments to test the entire scheme using U2OS (osteosarcoma) cells that expressed GFP. The laser power meter was used to measure the excitation light intensity at the sample plane and using the result shown in Fig. 3(a), we adjusted the LED DC current to produce $W_{sp} = 1.5$ mW of excitation light into each sample. This excitation power level was sufficient to produce high-quality images suitable for lifetime measurements. This value is significantly below the value of 94 mW in Table 1 because we did not try to extract the maximum number of photons from the GFP molecules. We also used an exposure time of 20 ms instead of the 200 ms in Table 1. We used the Olympus/LIFA system described in Sec. 3.1 with the 20× Zeiss objective lens with an NA = 0.5. For each cell, two images were acquired for the reasons described in Sec. 3.5.3. In each pair of cell images, a sample region was chosen. We then measured the SNR in that region. For each cell, we subtracted the contribution of the background variance from the total variance before we calculated the SNR per cell region. Our results are shown in Table 3.

The predicted SNR value is higher than the highest measured value by a factor of seven. The predicted value, however, was based upon the SNR that could be achieved if every single molecule in a pixel were illuminated until it had produced the *maximum* number of emission photons. This was not the case in our experiment. The samples we used were still very much "alive" after the images were recorded, that is, they were capable of producing more GFP emission photons.

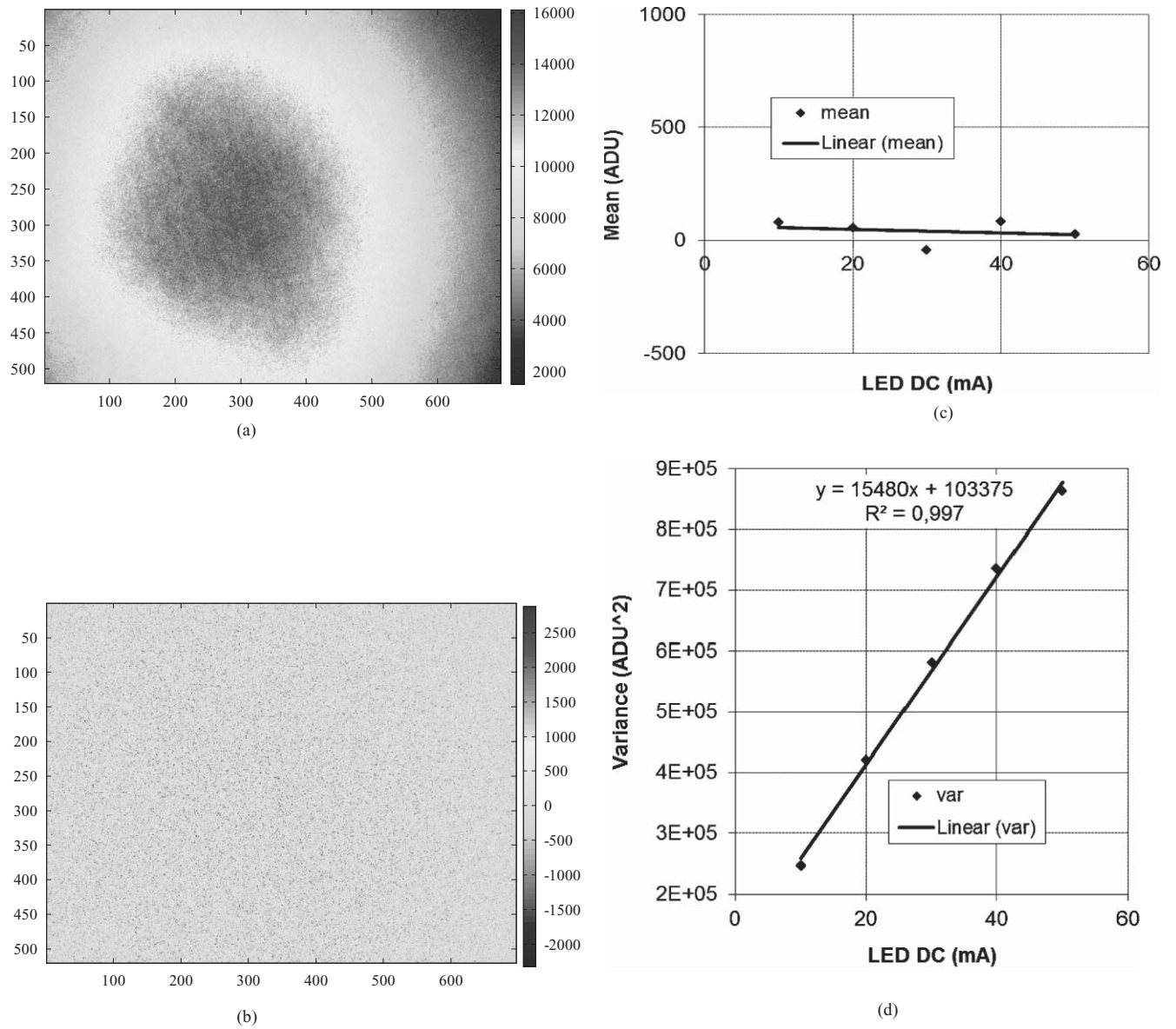

Fig. 5 Poisson noise validation for the detected fluorescence emission light. (a) Single image taken from the green fluorescent plastic test slide at 10 mA; (b) difference of the two "noise" images each acquired at 10 mA; (c) mean value of the difference images as a function of LED DC current varying from 10 to 50 mA; and (d) variance of the difference images as a function of LED DC current varying from 10 to 50 mA. It is this linearity that is indicative of the photon limited (Poisson) characteristic of the noise.

Table 3 Measurement results for U2OS cells expressing GFP. Experimental parameters were $\lambda_{ex} = 469$ nm, NA = 0.5, $n = 1.0$, $T = 20$ ms, and optical excitation power at sample $W_{sp} = 1.5$ mW. The predicted SNR is based upon Eq. (20).

Sample	Number of pixels	Average/pixel	Measured SNR/pixel	Predicted SNR/pixel
GFP slide - background	10 × 10	100.2	10.01 : 1 (20.0 dB)	
GFP slide – low intensity cell	10 × 10	167.3	12.93 : 1 (22.2 dB)	
GFP slide – middle intensity cell	10 × 10	759.7	27.56 : 1 (28.8 dB)	
GFP slide – high intensity cell	10 × 10	3746.9	61.21 : 1 (35.7 dB)	423 : 1 (52.5 dB)

Table 4 Names, units, values, and definitions of 41 parameters that are used in this paper. The values are taken from the fluorescein example developed in this paper.

Parameter	Units	Manuscript value	Meaning
λ_{ex}	[nm]	494	peak excitation wavelength
λ_{em}	[nm]	525	peak emission wavelength
τ_θ	[ns]	4.1	fluorescence lifetime measured from phase shift
τ_m	[ns]	4.1	fluorescence lifetime measured from modulation depth
V	[μm^3]	0.01	volume of one voxel
b	[μm]	25	linear size of one square pixel
a	–	512	number of pixels in row of square CCD image
M	–	100×	magnification of objective lens
n	–	1.51	refractive index of immersion medium
NA	–	1.3	numerical aperture of objective lens
Δz	[nm]	147	depth-of-field
c	[mol/m^3]	0.2×10^{-3}	molecule concentration (in moles)
m	[molecules/voxel]	11	molecules per voxel
T	[s]	0.2	exposure time of one image
T_0	[s]	0	time interval between two exposures with excitation illumination left on
r	–	12	number of (FLIM phase) images to be recorded
n_{emit}	–	30000	maximum number of photons/molecule emitted before photobleaching
n_{rec}	–	27,500	number of photons/recording/voxel before photobleaching
Φ	–	90%	(emitted photos)/(absorbed photons)
n_{absorb}	–	30,556	number of absorbed photons/recording/voxel before photobleaching
$\varepsilon(\lambda_{ex})$	[m^2/mol] or [M^{-1}cm^{-1}]	59668	molar extinction coefficient
n_0	–	7.6×10^9	number of excitation photons required to produce a given number of absorbed photons
$R_D(\lambda)$	–	95%	reflection coefficient of the dichroic mirror
$\tau_{EF}(\lambda)$	–	95%	transmission coefficient of the excitation filter
$\tau_{lens}(\lambda)$	–	96%	transmission coefficient of a lens in the excitation path
E_{ex}	[J/photon] or [eV/photon]	4.1×10^{-19} or 2.54	energy per photon from excitation source
W	[milliWatts]	5	optical power of excitation light source
W_{sp}	[milliWatts]	4.3	optical power of excitation light source at sample plane
SNR	ratio or [dB]	5:1 or (14)	signal-to-noise ratio after digitization
θ	[radians] or [°]	1.03 or 59°	half of the acceptance angle of objective lens
n_{epr}	–	2500	usable photons/recording/molecule

Table 4 (Continued.)

Parameter	Units	Manuscript value	Meaning
n_{lens}	–	625	number of photons that are collected by the objective lens/recording/molecule
γ	–	25%	% of emitted photons captured by objective lens
$\tau_{D(\lambda)}$	–	90%	transmission coefficient of the dichroic mirror
$\tau_{B(\lambda)}$	–	95%	transmission coefficient of the barrier filter
$\tau_{W(\lambda)}$	–	96%	transmission coefficient of the camera window
F	–	40%	camera fill factor
$\eta(\lambda)$	–	30%	quantum efficiency of the camera
κ	–	50%	area of CCD/area of illumination field
n_e	–	27	number of photoelectrons/molecule/recording
g	[ADU/e^-]	0.126	digital gray levels/photoelectron

Further, the wavelength dependence of the emitted photons and the assumption of wavelength constancy for various components, as described in Eq. (19), can lead to an overestimate for the predicted SNR. Approximately 39% of the GFP photons, for example, have a wavelength outside the previously indicated (λ_1, λ_2) interval. Together, these two effects (less-than-maximum photon production and wavelength dependency), can explain the lower-than-predicted, measured SNR.

More importantly, with this amount of illumination delivered to the sample, the intensity values we measured were compatible not only with ordinary widefield fluorescence digital imaging but also with the requirements for lifetime imaging. Using the LIFA system and $W_{sp} = 1.6$ mW of optical excitation power, we measured a fluorescence lifetime for the GFP in the U2OS cells of $\tau_\theta = 2.17 \pm 0.14$ ns. This favorably compares with lifetime values around 2.1 ns reported in literature[49] and shows that at this excitation power level, a precision (CV) of 6.5% can be achieved in the measurement of the lifetime. These results demonstrate that our predictions over the entire system (from light source to digital image) are supported by these data.

5 Conclusions

A quantitative analysis has been made of the photon budget in a FLIM system. This concept is relevant to many fluorescence microscope users and the formulas are not restricted to FLIM but applicable to widefield fluorescence microscopy in general. For widefield fluorescence microscopy values to be determined, we need only set $r = 1$ in the various equations to determine the required excitation source power and the resulting SNR in the image. A light source of only a few milliWatts is sufficient for a FLIM system using fluorescein as an example. For every 100 photons emitted, around one photon will be converted to a photoelectron, leading to an estimate for the ideal SNR for one fluorescein molecule in an image as 5 (14 dB). The SNR for a single pixel and for the whole image with the molecule concentration of 2 μM are 18 (25 dB) and 9000 (79 dB), respectively. At this SNR, the need for EM readout for a CCD camera system is dubious. But, as previously mentioned, for any of a number of reasons (a weaker excitation source, a lower quantum yield or molar extinction coefficient, or a reduction in CCD sensitivity), the SNR could decrease, which would mean that EM readout would be beneficial. Calculations of other fluorophores are also given as examples, such as Fura-2, GFP, EYFP, Rhodamine 6G, Alexa-546, Cy3, tetramethylrhodamine, and Cy5.

We have performed experiments to validate the parameters and assumptions used in the mathematical model. The transmission efficiency of the lenses, filters, and mirrors in the optical chain can be treated as a single constant parameter. The Beer-Lambert law is applicable to obtain the absorption factor in the mathematical model. The Poisson distribution assumption used in deducing the SNR is also valid. This quantitative analysis provides a framework for the design and fabrication of current and future fluorescence lifetime imaging microscope systems.

In this paper, we have defined and used a large number of parameters, which are summarized in Table 4 together with their units, typical values (as used in this manuscript), and definitions.

6 Future Work

In a future paper we will examine the estimation of fluorescence parameters, such as lifetime as a function of SNR and sample heterogeneity. As in this paper, results will be based upon a mathematical model and experimental results, but with the addition of simulations.

Considering the results obtained from the mathematical model and with the help of the simulation package, we are working on building a new type of FLIM system. The current implementation of frequency-domain FLIM requires an image intensifier based on a micro-channel plate (MCP).[20] This conventional system has room for improvement and a robust solid-state camera would present a desirable alternative to MCPs.[50,51]

We are, therefore, designing and building a CCD image sensor that can be modulated at the pixel level.

The proposed FLIM system should have the following advantages: 1. there will be no need for a high voltage source, 2. the entire signal will be used during demodulation, 3. spatial resolution will be limited only by optics and pixel dimensions, 4. there will be no geometric distortion, and 5. as we have become accustomed with solid-state devices, it will be compact and of relatively low cost.

Acknowledgments

The authors would like to thank DALSA Professional Imaging, Eindhoven, The Netherlands and The Netherlands Cancer Institute, Amsterdam, The Netherlands for their collaboration in this project. Funding from Innovation-Oriented Research Program (IOP) of The Netherlands (IPD083412A) is gratefully acknowledged. We thank Professor Dorus Gadella and the people in his lab at the University of Amsterdam for helping us with lifetime calibration and Dr. Vered Raz of the Leiden University Medical Center for providing us with the U2OS cells.

References

1. A. Esposito, H. C. Gerritsen, and F. S. Wouters, "Fluorescence lifetime imaging microscopy quality assessment and standard," *Springer Series on Fluorescence* **6**, 117–142 (2008).
2. A. Squire, P. J. Verveer, and P. I. H. Bastiaens, "Multiple frequency fluorescence lifetime microscopy," *J. Microsc.* **197**, 136–149 (2000).
3. M. W. Conklin, P. P. Provenzano, K. W. Eliceiri, R. Sullivan, and P. J. Keely, "Fluorescence lifetime imaging of endogenous fluorophores in histopathology sections reveals differences between normal and tumor epithelium in carcinoma in situ of the breast,"*Cell Biochem. Biophys.* **53**, 145–157 (2009).
4. S. E. D. Webb, S. Lévêque-Fort, D. S. Elson, J. Siegel, T. Watson, M. J. Lever, M. Booth, R. Juskaitis, M. A. A. Neil, L. O. Sucharov, T. Wilson, and P. M. W. French, "Wavelength-resolved 3-dimensional fluorescence lifetime imaging," *J. Fluoresc.* **12**, 279–283 (2004).
5. K. Carlsson, A. Liljeborg, R. M. Andersson, and H. Brismar, "Confocal PH imaging of microscopic specimens using fluorescence lifetimes and phase fluorometry: influence of parameter choice on system performance," *J. Microsc.* **199**, 106–114 (2000).
6. A. Squire and P. I. H. Bastiaens, "Three dimensional image restoration in fluorescence lifetime imaging microscopy," *J. Microsc.* **193**, 36–49 (1999).
7. T. French, P. T. C. So, D. J. Weaver, T. Coelho-Sampaio, and E. Gratton, "Two-photon fluorescence lifetime imaging microscopy of macrophage-mediated antigen processing," *J. Microsc.* **185**, 339–353 (1997).
8. K. Suhling, P. M. W. French, and D. Phillips, "Time-resolved fluorescence microscopy," *Photochem. Photobiol. Sci.* **4**, 13–22 (2005).
9. G. Marriott, R. M. Clegg, D. J. Arndt-Jovin, and T. M. Jovin, "Time resolved imaging microscopy," *Biophys. J.* **60**, 1374–1387 (1991).
10. S. Brustlein, F. Devaux, and E. Lantz, "Picosecond fluorescence lifetime imaging by parametric image amplification," *European Phys. J.: Appl. Phys.* **29**, 161–165 (2005).
11. T. W. J. Gadella, Jr., A. van Hoek, and A. J. M. G. Visser, "Construction and characterization of a frequency-domain fluorescence lifetime imaging microscopy system," *J. Fluoresc.* **7**, 35–43 (1997).
12. P. J. Verveer, A. Squire, and P. I. H. Bastiaens, "Global analysis of fluorescence lifetime imaging microscopy data," *Biophys. J.* **78**, 2127–2137 (2000).
13. O. Holub, M. J. Seufferheld, C. Gohlke, Govindjee, and R. M. Clegg, "Fluorescence lifetime imaging (FLI) in real-time - a new technique in photosynthesis research," *Photosynth. Res.* **38**, 581–599 (2000).
14. A. Elder, S. Schlachter, and C. F. Kaminski, "Theoretical investigation of the photon efficiency in frequency-domain fluorescence lifetime imaging microscopy," *J. Opt. Soc. Am. A* **25**, 452–462 (2008).
15. A. Esposito, H. C. Gerritsen, and F. S. Wouters, "Optimizing frequency-domain fluorescence lifetime sensing for high-throughput applications photon economy and acquisition speed," *J. Opt. Soc. Am. A* **24**, 3261–3273 (2007).
16. J. Philip and K. Carlsson, "Theoretical investigation of the signal-to-noise ratio in fluorescence lifetime imaging," *J. Opt. Soc. Am. A* **20**, 368–379 (2003).
17. H. C. Gerritsen, M. A. H. Asselbergs, A. V. Agronskaia, and W. G. J. H. M. Van Sark, "Fluorescence lifetime imaging in scanning microscopes: acquisition speed, photon economy and lifetime resolution," *J. Microsc.* **206**, 218–224 (2002).
18. Q. Zhao, I. T. Young, and J. G. S. de Jong, "Photon budget analysis for a novel fluorescence lifetime imaging microscopy system with a modulated electron-multiplied all-solid-state camera," in *Proc. of IEEE Nanomed Conf.*, pp. 25–26, Tainan, Taiwan (2009).
19. Q. Zhao, I. T. Young, and J. G. S. de Jong, "Where did my photons go?-Analyzing the measurement precision of FLIM," in *Proc. of Focus on Microscopy 2010 Conf.*, pp. 132, Shanghai, China (2010).
20. R. M. Clegg, "Fluorescence lifetime-resolved imaging: what, why, how-a prologue," in *FLIM Microscopy in Biology and Medicine*, A. Periasamy and R. M. Clegg, Eds., pp. 3–29, CRC Press, Boca Raton (2009).
21. I. T. Young, "Image fidelity: characterizing the imaging transfer function," in *Fluorescence Microscopy of Living Cells in Culture-Part B*, D. L. Taylor and Y. L. Wang, Eds., pp. 2–45, Academic Press, San Diego (1989).
22. A. C. Mitchell, J. E. Wall, J. G. Murray, and C. G. Morgan, "Direct modulation of the effective sensitivity of a CCD detector: a new approach to time-resolved fluorescence imaging," *J. Microsc.* **206**, 225–232 (2002).
23. E. B. van Munster and T. W. J. Gadella, Jr., "Suppression of photobleaching-induced artifacts in frequency-domain FLIM by permutation of the recording order," *Cytometry, Part A* **58A**, 185–194 (2004).
24. M. Born, and E. Wolf, *Principles of Optics*, 6th ed., Pergamon, London, pp. 435–442 (1980).
25. A. Diaspro, G. Chirico, C. Usai, P. Ramoino and J. Dobrucki, "Photobleaching," in *Handbook of Biological Confocal Microscopy*, J. B. Pawley, Eds., pp. 690–702, Springer Science + Business Media, New York, 2006.
26. J. C. Mullikin, L. J. v. Vliet, H. Netten, F. R. Boddeke, G. v. d. Feltz, and I. T. Young, "Methods for CCD camera characterization," *Proc. SPIE* **2173**, 73–74 (1994).
27. I. T. Young, J. J. Gerbrands, and L. J. v. Vliet, "Image processing fundamentals," in *The Digital Signal Processing Handbook*, V. K. Madisetti and D. B. Williams, Eds., pp. 51.1–51.81, CRC Press, Boca Raton, Florida (1998).
28. http://omlc.ogi.edu/spectra/PhotochemCAD/abs_html/fluorescein-dibase.html.
29. R. P. Haugland, "Fluorescent labels," in *Biosensors with Fiber Optics*, D. L. Wise, L. B. Wingard, Eds., pp. 85–108, Humana, Clifton (1991).
30. http://www.semrock.com/Catalog/SetDetails.aspx?SetBasePartID=11.
31. P. L. Becker and F. S. Fay, "Photobleaching of Fura-2 and its effect on determination of calcium concentrations," *Am. J. Physiol.* **253**, C613–C618 (1987).
32. G. Grynkiewicz, M. Peonie, and R. Y. Tsien, "A new generation of Ca2 + indicators with greatly improved fluorescence properties," *J. Biol. Chem.* **260**, 3440–3450 (1985).
33. U. Kubitscheck, O. Kückmann, T. Kues, and R. Peters, "Imaging and tracking of single GFP molecules in solution," *Biophys. J.* **78**, 2170–2179 (2000).
34. D. M Chudakov, V. V Verkhusha, D. B Staroverov, E. A Souslova, S. Lukyanov, and K. A Lukyanov, "Photoswitchable cyan fluorescent protein for protein tracking," *Nat. Biotechnol.* **22**, 1435–1439 (2004).
35. http://flowcyt.salk.edu/fluo.html.
36. S. Ganesan, S. M. Ameer-beg, T. T. C. Ng, B. Vojnovic, and F. S. Wouters, "A dark yellow fluorescent protein (YFP)-based resonance energy-accepting chromoprotein (REACh) for Förster resonance energy transfer with GFP," *Proc. Natl. Acad. Sci. U.S.A.* **103**, 4089–4094 (2006).

37. A. Renn, J. Seelig and V. Sandoghdar, "Oxygen-dependent photochemistry of fluorescent dyes," *Mol. Phys.* **104**, 409–414 (2006).
38. P. K. Jain, K. S. Lee, I. H. El-Sayed, and M. A. El-Sayed, "Calculated absorption and scattering properties of gold nanoparticles of different size, shape, and composition: applications in biological imaging and biomedicine," *J. Phys. Chem. B* **110**, 7238–7248 (2006).
39. R. F. Kubin and A. N. Fletcher, "Fluorescence quantum yields of some rhodamine dyes," *J. Lumin.* **27**, 455–462 (1982).
40. G. Horváth, M. Petrás, G. Szentesi, Á. Fábián, J. W. Park, G. Vereb, and J. Szöllös, "Selecting the right fluorophores and flow cytometer for fluorescence resonance energy transfer measurements," *Cytometry, Part A* **65A**, 148–157 (2005).
41. S. R. Mujumdar, R. B. Mujumdar, C. M. Grant, and A. S. Waggoner, "Cyanine-labeling reagents: sulfobenzindocyanine succinimidyl," *Bioconjugate Chem.* **7**, 356–362 (1996).
42. S. Kenmoku, Y. Urano, H. Kojima, and T. Nagano, "Development of a highly specific rhodamine-based fluorescence probe for hypochlorous acid and its application to real-time imaging of phagocytosis," *J. Am. Chem. Soc.* **129**, 7313–7318 (2007).
43. http://thesis.library.caltech.edu/1693/5/chapter5_spectro.pdf.
44. E. Füreder-Kitzmüller, J. Hesse, A. Ebner, H. J. Gruber and G. J. Schütz, "Non-exponential bleaching of single bioconjugated Cy5 Molecules," *Chem. Phys. Lett.* **404**, 13–18 (2005).
45. J. B. Jensen, L. H. Pedersen, P. E. Hoiby, L. B. Nielsen, T. P. Hansen, J. R. Folkenberg, J. Riishede, D. Noordegraaf, K. Nielsen, A. Carlsen, and A. Bjarklev, "Photonic crystal fiber based evanescent-wave sensor for detection of biomolecules in aqueous solutions," *Opt. Lett.* **29**, 1974–1976 (2004).
46. M. S. Robbins, "Electron multiplying CCDs," *5th Fraunhofer IMS Workshop*, Duisburg, Germany (2010).
47. http://www.sciencegateway.org/resources/fae1.htm.
48. http://www.andor.com/learning/digital_cameras/?docid=315.
49. V. Ghukasyan, C.-R. Liu, F.-J. Kao, and T.-H. Cheng, "Fluorescence lifetime dynamics of enhanced green fluorescent protein in protein aggregates with expanded polyglutamine," *J. Biomed. Opt.* **15**(1), 1–11 (2010).
50. A. Esposito and F. S. Wouters, "Fluorescence lifetime imaging microscopy," in *Current Protocols in Cell Biology*, J. S. Bonifacino, M. Dasso, J. B. Harford, J. Lippincott-Schwartz, and K. M. Yamada, Eds., pp. 4.14.11–14.14.30, John Wiley & Sons, New York (2004).
51. A. Esposito, T. Oggier, H. C. Gerritsen, F. Lustenberger, and F. S. Wouters, "All-solid-state lock-in imaging for wide-field fluorescence lifetime sensing," *Opt. Express* **13**, 9812–9821 (2005).